MATERIALS PHYSICS AND MECHANICS RESEARCH ARTICLE

Submitted: November 24, 2023 **Revised: May 21, 2024** **Accepted: August 28, 2024**

Synthesis of $WO_{2.72}$:Fe thin films via ammonium tungstate precursor by spray pyrolysis technique and annealing

E. Ouadah, N. Hamdadou ✉,

Laboratoire de Micro et de Nanophysique, Ecole Nationale Polytechnique d'Oran, Oran, Algérie

✉ nasreddine.hamdadou@enp-oran.dz

ABSTRACT

In this study, $WO_{2.72}$:Fe thin films have been prepared on glass substrates heated to a fixed temperature of 350 °C by the spray pyrolysis technique, from an aqueous ammonium tungstate solution $(NH_4)_{10}H_2(W_2O_7)_6$ with a concentration of 0.005 M. The dopant concentrations were 1, 3 and 5 %. After deposition, the thin films were annealed at 550 °C for 4 h. The characterization results revealed that Fe doping has a significant effect on the morphology of thin films depending on its concentration. In addition, it promotes crystallites growth and improves the surface quality. GIXRD analysis has shown that the thin films obtained after the annealing are polycrystalline in nature, the structure of the $WO_{2.72}$ films was monoclinic, with space groups P2/m (10). The growth direction was variable depending on the doping concentration. It was noticed that the peaks positions, the preferential grain orientation and the structural parameters are affected by the doping concentrations, which had no effect on the phase type of the obtained films. The $WO_{2.72}$ films have interesting optical properties; high transmittance in the visible range of 75 % as well as high absorption in the ultra-violet range from 1.4 to 0.2 a.u. Moreover, the films exhibit both direct and indirect electronic transitions, which are red-shifted due to Fe-doping.

KEYWORDS

$WO_{2.72}$ thin film • spray pyrolysis • Fe-doping • roughness • GIXRD • spectrophotometry

Citation: Ouadah E, Hamdadou N. Synthesis of $WO_{2.72}$:Fe thin films via ammonium tungstate precursor by spray pyrolysis technique and annealing. *Materials Physics and Mechanics*. 2024;52(4): 141–151. http://dx.doi.org/10.18149/MPM.5242024_12

Introduction

WO_x tungsten oxides are n-type wide band gap semiconductor (2.5 – 3.6 eV), and can easily be produced as thin films with high optical transparency in the visible range. These materials allow us to use its in many applications such as: solar energy conversion, semiconductor gas sensors, photocatalysis, electrochemical screens and field emission devices FED [1,2]. Among the different phases of tungsten oxides, non-stoichiometric tungsten oxides WO_{3-x}, $x < 3$ are important due to oxygen vacancy defects [3,4]. Particularly in recent years, the nanomaterials of $WO_{2.72}$ have attracted the attention of several works because they have excellent properties for nanotechnology applications [5]. In addition, $WO_{2.72}$ with monoclinic structure is the poorest in oxygen among non-stoichiometric tungsten oxide materials [6]. They have presented various morphologies like nanospheres, nanowires, nanofibers and sea urchin-shaped nanostructures [6]. Several preparation techniques have been used to prepare $WO_{2.72}$ thin films, including thermal evaporation of tungsten oxide [7], solvothermal techniques [8], physical vapor deposition PVD, sol-gel process, the electrochemical technique and chemical vapor deposition CVD [9], spray pyrolysis technique [10]. Several works have been carried out on the nanorods and the nanowires of $WO_{2.72}$ [11,12].

Publisher: Peter the Great St. Petersburg Polytechnic University

In this work, we have used the reactive chemical spraying technique in liquid phase (spray pyrolysis) for the preparation of $WO_{2.72}$ thin films, because it's simple, economical with a high growth rate and even the injection of dopants is without any difficulty. The obtained thin films have been annealed at 550 °C for 4 hours. To improve the physical and chemical properties of the $WO_{2.72}$ thin films, several dopants have been used such as Ti, Fe [13,14], Al [15], Mo [16], Ce and La [17,18]. We have chosen the Fe element as a dopant with doping concentrations 1, 3 and 5 %, because it has an important role in reducing the band gap of $WO_{2.72}$.

Experimental details

Thin films preparation

$WO_{2.72}$ thin films were deposited on glass substrates of dimensions 26 × 10 × 1 mm at constant temperature of 350 °C by spray-pyrolysis using a HOLMARC brand. The glass substrates were cleaned previously in an ultrasonic bath with acetone and ethanol three times for 5 min; then, with deionized water to remove traces of microscopic impurities.

The precursor solution of 0.005 M was prepared from ammonium tungstate $(NH_4)_{10}H_2(W_2O_7)_6$ dissolved in 100 ml of deionized water. After that, the solution was sprayed using a syringe-attached sprayer. The air-directed spray stream has been used as a carrier gas. The substrate-nozzle distance and the spraying rate were 12 cm and 200 µl/min, respectively, with an air pressure of 1.5 bar. The deposition time was 8 min.

The Fe dopant concentration was 1, 3 and 5 at. %. After cooling to room temperature, the films were annealed at 550 °C for 4 hours using a MAGMA THERM programmable tubular oven, with a heating rate of 10 °C/min. The purpose of this annealing is to improve the densification and crystallization. Table 1 depicts the deposition parameters of the films.

Table 1. Deposition parameters of $WO_{2.72}$:Fe thin films

Parameter	Value
Substrate	Glass
Substrate temperature, °C	350
Precursor volume, ml	20
Solvent	Deionized water
Dopant	Fe
Spray rate, µl/min	200
Nozzle-substrate distance, cm	12
Spray duration, min	8
Annealing temperature, °C	550
Annealing duration, h	4

Thin films characterization

The films thickness was measured using a Bruker Dektak XT profilometer, which also gives the roughness parameters of the surface. The data processing was carried-out by Vision 64 software. The structural properties were obtained by grazing incidence X-ray diffraction (GIXRD) using an INEL Equinox 3000 diffractometer operating in the range of 0–120° with a filtered Cu-Kα radiation (λ = 1.54056 Å). The data processing was

performed by Match 3 software. The optical transmittance and absorbance spectra were carried out at room temperature by a dual beam UV–Visible spectrophotometer Specord 210 Plus in the wavelength range of 300–1100 nm.

Results and Discussion

Film thickness and profile analysis

The surface profilometry is a non-destructive technique and allows studying the film profile. Several parameters are reliable to the surface roughness. Table 2 shows the primary profile Pp, the total profile Pt and the thickness e of $WO_{2.72}$:Fe films annealed at 550 °C for 4 h. It is observed that the surface primary and total profiles decrease with Fe-doping.

Table 2. Thickness, primary profile and total profile of $WO_{2.72}$:Fe thin films after annealing at 550 °C for 4 h

Parameter	Doping concentration, %		
	1	3	5
e, nm	352	396	245
P_P, Å	28108	12403	5624
P_t, Å	31275	13866	6214

Table 3. Surface profile parameters of $WO_{2.72}$:Fe films after annealing at 550 °C for 4 h

Parameter	Doping concentration, %		
	1	3	5
P_q, Å	2710.87	2747.67	759.65
P_{sk}	5.074	2.29	4.856
P_{ku}	40.52	7.397	27.362
P_z, Å	31275.04	13866.13	6214.45
P_v, Å	3166.71	1462.19	589.65

Furthermore, the other parameters such as the root mean square deviation of the assessed profile P_q, the skewness of the assessed profile P_{sk}, the kurtosis of the assessed profile P_{ku}, are gathered in Table 3. These parameters are often used to get insights on the surface quality. The assessed profile is characterized by three parameters, its maximum height P_z, its maximum profile peak height P_p, and its maximum profile valley depth P_v:

$$\begin{cases} P_q = [\frac{1}{l}\int_0^l Z^2(x)dx]^{1/2} \\ P_{\text{sk}} = \frac{1}{(P_{q_i})^3}[\frac{1}{l}\int_0^l Z^3(x)dx] \\ P_{\text{ku}} = \frac{1}{(P_{q_i})^4}[\frac{1}{l}\int_0^l Z^4(x)dx] \\ P_Z = P_P + P_V \\ P_v = \frac{1}{\text{CN}}\sum_{i=1}^{CN} Pv_i \end{cases}. \quad (1)$$

Figure 1 shows the variation of the surface profile parameters with Fe-doping concentration. It is observed that the parameters P_q, P_z, P_p and P_v decrease with increasing of the dopant concentration. Hence, Fe-doping improves the surface quality. It is evident that thermal treatment at higher temperatures promotes the growth of the crystallites and enhances the roughness of the surface.

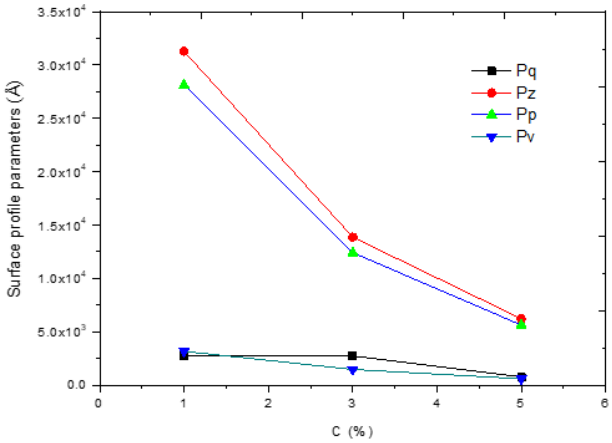

Fig. 1. Same surface profile parameters of $WO_{2.72}$:Fe thin films as a function of doping concentration

GIXRD analysis

Grazing incidence X-ray diffraction (GIXRD) technique was used to determine the structure, crystallographic growth directions, lattice parameters, and average grains size. Before annealing, the thin films are amorphous (Fig. 2(a)). Figure 2(b) shows the GIXRD patterns of $WO_{2.72}$:Fe films after annealing at 550 °C for 4 hours.

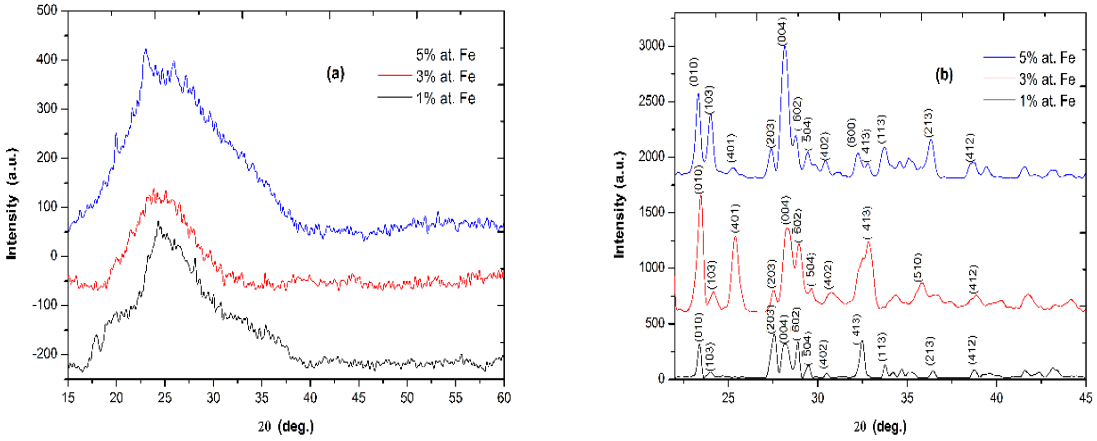

Fig. 2. GIXRD diagrams of $WO_{2.72}$:Fe films with different doping concentrations; before (a) and after (b) annealing at 550 °C for 4 hours

The thin films are of polycrystalline nature, all peaks appearing are attributed to $WO_{2.72}$ of monoclinic structure, identified using the ICDD card N°36-0101. No. Fe diffraction peak or other phases, is detected which indicates that the thin films are well crystallized. Table 4 indicates the Bragg angles θ, the relative intensities of the diffraction peaks and the Miller indices (*hkl*) for different doping concentrations. All the spectra of $WO_{2.72}$:Fe thin films represent the same peaks of the planes (103), $(\bar{6}02)$, $(\bar{5}04)$, (402), $(\bar{4}13)$ and (412) which are considerably lower and wider peaks, but the most intense peak was attributed to the orientations (203), (010) and (004), with doping concentrations 1, 3 and 5 %, respectively. Usually, the sharp diffraction peaks require the lowest formation energy. In addition, with an increase in the doping concentration 1, 3 and 5 %, the grains preferential orientation changes from (203), (010) and (004), respectively,

indicating a change in the growth mechanism of these thin films, from a direction parallel to the surface of the substrate (010) to a perpendicular direction (004). The peak at orientation (010) is attributed to $WO_{2.72}$ of monoclinic structure as reported in previous works [19], the diffraction angles corresponding to this orientation with doping concentrations at 1, 3 and 5 % were 23.49°, 23.37° and 23.34°, respectively. These results show slight shifts of this diffraction peak towards lower angles. This suggests that the crystal structure is modified during Fe doping due to the very similar ion radius of Fe and W ions [20]. In addition, the incorporation of Fe doesn't change the phase type of $WO_{2.72}$ and no new peak has appeared, indicating the Fe homogeneous incorporation into the lattice of $WO_{2.72}$ [20].

Table 4. The peak positions, the relative intensities and the Miller indices of $WO_{2.72}$:Fe thin films for different doping concentrations

1 %		3 %		5 %		(*hkl*)
2θ, deg.	I, %	2θ, deg.	I, %	2θ, deg.	I, %	
23.49	77	23.37	100	23.34	86	(010)
24.12	17	24.08	47	24.03	80	(103)
27.67	100	27.44	48	27.42	69	(203)
28.29	77	28.36	82	28.19	100	(004)
28.99	82	28.87	74	28.79	73	$(\bar{6}02)$
29.58	30	29.55	49	29.46	68	$(\bar{5}04)$
30.61	13	30.67	47	30.46	66	(402)
32.59	86	32.76	75	32.82	65	$(\bar{4}13)$
38.86	21	38.79	46	38.72	65	(412)

The lattice parameters have been deduced using the relations below:

$$\begin{cases} \frac{1}{d_{hkl}^2} = \frac{1}{\cos^2\beta}\left(\frac{h^2}{a^2} + \frac{k^2\sin^2\beta}{b^2} + \frac{l^2}{c^2} - \frac{2hk\cos\beta}{ab}\right) \\ d_{hkl} = \frac{\lambda}{2\sin\theta} \end{cases}, \quad (2)$$

where d_{hkl} is the inter-reticular distance.

The *FWHM* (Full Width at Half Maximum) of the peaks were calculated by Warren relation:

$$(FWHM)^2 = B^2 - b^2, \quad (3)$$

where *B* is the observed widening, which is given directly by the data processing software of the diffractometer and *b* is instrumental broadening which is equal to 0.08° in our case.

The average grain size *D* was determined using Scherrer formula [21]:

$$D = 0.9\frac{\lambda}{FWHM.\cos\theta}, \quad (4)$$

where λ is the X-rays wavelength. Table 5 indicates the lattice parameters *a*, *b*, *c* and β, the full width at half maximum *FWHM* of the most intense peak, the average grain size *D*, the unit cell volume V, the lattice strain ε and the dislocation density *δ*.

The *FWHM* of the most intense peaks decreased with the increase in the dopant level up to about 3 % at first, which implies an increase in the grain size and improved crystal quality (Table 5). Tungsten typically exists in the +6 (W^{+6}) oxidation state. When iron, which can be in the +2 (Fe^{+2}) or +3 (Fe^{+3}) oxidation state, is introduced, a charge imbalance occurs, resulting in electrostatic instability. To restore this balance within the crystal structure, oxygen atoms may be released, creating oxygen vacancies. The charge difference between tungsten and iron ions provides the energy needed for these

vacancies to form. These vacancies serve as low-energy active sites, around which atoms can cluster to form larger and more uniform crystalline grains. Thus, increasing the number of oxygen vacancies can enhance the size and regularity of the crystalline grains [22], which is considered very beneficial for gas detection application. In addition, the presence of oxygen vacancies would generally give the material better conductivity [23]. On the other hand, beyond 3 %, there is an increase in the *FWHM* of the peaks, which is reflected by deterioration in the crystal quality and a reduction in the grain size, or this leads to a significant increase in the specific surface area of grain boundaries [16]. In addition, the change in the grain size depends on the change in the density of the nucleation centers, created just at the time of thin film growth. The greater the density of the nucleation centers, the smaller the grain size and vice versa.

Table 5. Structural parameters values of $WO_{2.72}$:Fe thin films after annealing at 550 °C for 4 h: the lattice parameters *a*, *b*, *c* and β, FWHM is the full width at half maximum of the most intense peak, D is the grain size, V is the unit cell volume, ε is the lattice strain, δ is the dislocation density

Fe-doping, %	Lattice parameter				FWHM, deg.	D, nm	V, Å^3	ε, × 10^{-3}	δ, lines/μm^2
	a, Å	b, Å	c, Å	β, °					
1	19.8952	3.7830	14.4234	119.06	0.23962	33.92	424.9	1.02	869.1
3	18.6829	3.8018	14.0615	116.58	0.17943	45.31	428.3	0.76	487.1
5	18.7784	3.8068	14.2880	117.69	0.23904	34.00	456.9	1.02	865.0

It can be seen in Table 5 that the lattice parameters are varied with increasing Fe concentration. This variation may be attributed to the incorporation of Fe^{3+} ions into the system of $WO_{2.72}$:Fe because the Fe^{3+} ion can perform the same coordination as that of W^{6+}.

The dislocation density δ of the film defines the length of the dislocation lines per crystal volume unit. This parameter was calculated using the following relation:

$$\delta = \frac{1}{D^2}, \quad (5)$$

where *D* is the average grain size evaluated from the XRD data. The cell deformation varies proportionally with the stress, which is the resultant of the internal forces in matter. The strain *ε* in the studied films was evaluated using the following equation:

$$\varepsilon = \frac{FWHM\ cos\ \theta}{4}. \quad (6)$$

Table 5 shows the results of stain variation and dislocation density of thin films of $WO_{2.72}$:Fe for different doping concentrations. Strain and dislocation density decrease with increasing dopant concentration from 1 to 3 %, then increase for the dopant concentration from 3 to 5 %, these results agree well with the variation observed in the grain size. The smaller dislocation density values for the doped thin films indicate the homogeneous nucleation growth in the formation of $WO_{2.72}$ thin films, the reduction of the lattice imperfections concentration and the formation of thin films with high crystallinity. Consequently, these observations confirmed that the increase in the grain size is linked to the reduction in deformation and therefore to the reduction in the dislocation density in these films. Moreover, when iron is incorporated into the thin films of $WO_{2.72}$, it can substitute for tungsten atoms in the crystal lattice. This substitution leads to the formation of new equilibrium sites within the lattice, which helps reorganize the network to achieve greater stability. So, iron doping can also contribute to the redistribution of stresses arising from tungsten defects, thereby reducing distortions [24,25].

Optical analysis

The spectrophotometry measurements were performed at room temperature. With the increase in the wavelength, Fig. 3(a) shows a strong decrease in absorption in the ultraviolet from 1.4 to 0.2 a.u. and an average decrease in the visible range from 0.2 to 0.1 a.u. There is no absorption band in the visible region. It can be seen that the prepared thin films had a much higher absorption capacity in the ultraviolet region than in the visible region, which should behave as a UV protective material, which is in good agreement with the result reported by Morankar PJ et al. [16], and similar results were also found for the tungsten bronze compounds of Cs_xWO_3 and K_xWO_3 [26]. On the other hand, the thin films of $WO_{2.72}$:Fe doped at 1 % have the lowest absorbance in the visible region, on the other hand, the highest absorbance was observed for those doped at 5 %.

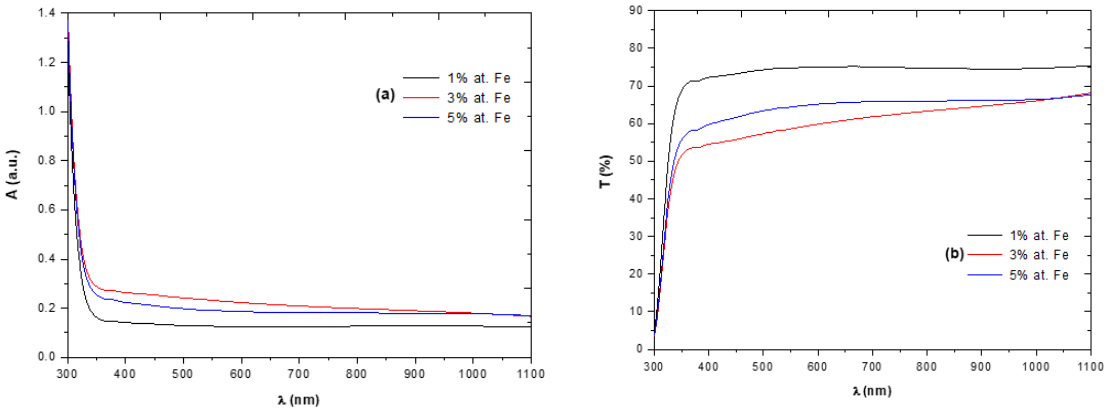

Fig. 3. Absorbance (a) and transmittance spectra (b) of $WO_{2.72}$:Fe thin films

The transmittance of a thin film is influenced by factors such as surface roughness, scattering of grain boundaries, optical inhomogeneity, etc. From Fig. 3(b), we can notice that, the $WO_{2.72}$:Fe thin films having a higher transmittance in the visible range, on the other hand, in the ultraviolet range it is weaker. That is why we can say that the $WO_{2.72}$:Fe thin films have an optical selectivity, because it reaches different optical transmittance for the visible region and the ultraviolet region, of which the $WO_{2.72}$ thin films give an interesting optical characteristic, thus, it can transmit most of the Vis light and mask almost all of the UV light [27], and similar results have been found in the UV-Vis domain for the $WO_{2.72}$ bulk [11,12], $K_xWO_{3+x/2}$ [26] and the tungsten bronze compounds of Cs_xWO_3 and K_xWO_3 [26]. As a consequence, the $WO_{2.72}$:Fe thin films can be used as sun filters in the UV-Vis range. In addition, the transmittance of thin films doped at 1 % reaches the greatest value 75 % in the visible domain and decreases to 68 and 67 % with the increase in doping concentration from 3 to 5 % respectively, this decrease can be attributed to the propagation losses at the grain's boundaries and oxygen vacancies. When introducing iron (Fe) as a dopant into $WO_{2.72}$ material, it leads to the formation of "impurity energy levels" or "defect levels" within the original energy bandgap of the material. When light with appropriate energy strikes this material, it is absorbed more effectively due to the transfer of this required energy to the newly formed energy levels. This enhances the absorption of light in certain energy ranges and reduces the optical transmittance in the visible region [28].

The absorption coefficient α was calculated from the transmission data using the equation:

$$\alpha = \frac{1}{e} ln(\frac{100}{T}), \quad (7)$$

where e represents the thickness (cm) and T is the optical transmittance (%).

Figure 4 shows the variation of the optical absorption coefficient of $WO_{2.72}$:Fe thin films. The optical absorption coefficient values reached ~ 0.64 10^4, ~ 0.81 10^4 and ~ 2.32 10^4 cm^{-1} for the doping concentrations 1, 3 and 5 % respectively. In other words, they increase proportionally with the doping concentration. This confirms that doping has an effect on the optical absorption coefficient.

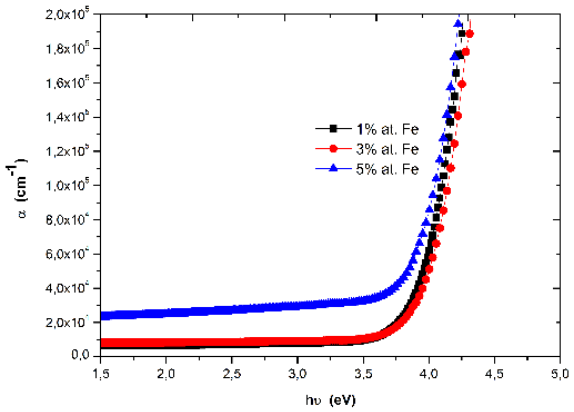

Fig. 4. Variation of the optical absorption coefficient of $WO_{2.72}$:Fe thin films

To determine the band gap energy, we have used Tauc formula, which is given as follow [29]:

$$\alpha h\upsilon = A(h\upsilon - E_g)^n, \quad (8)$$

where A is a constant, h is the Planck constant, v is the frequency of the incident light. The constant n = 1/2 in the case of a direct optical transition and n = 2 in the case of an indirect optical transition. E_g is deduced from the plot $(\alpha hv)^2 = f(hv)$ by linear extrapolation to the abscissa axis.

Figures 5(a) and 5(b) show the plots for direct and indirect allowed optical transitions in the thin films, respectively.

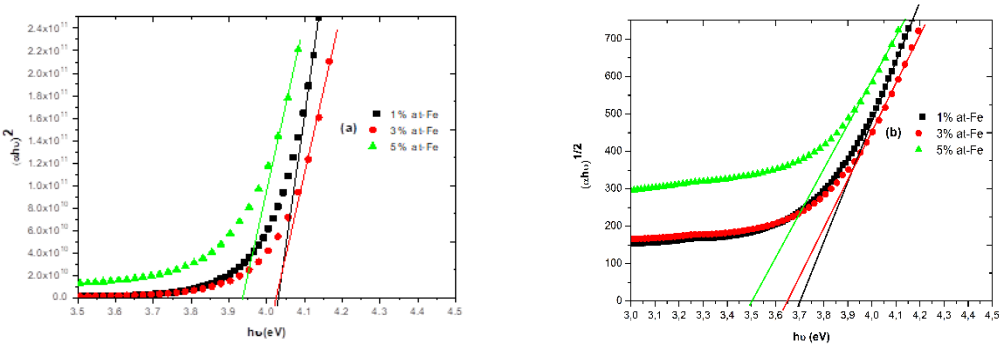

Fig. 5. Direct (a) and indirect (b) optical transitions of $WO_{2.72}$:Fe thin films

The extrapolation of the linear parts of these curves yields the value of the optical band gap (E_g^I is the direct optical band gap, E_g^{II} is the indirect optical band gap). Table 6 resumes the obtained values for $WO_{2.72}$:Fe thin films. The band gap energy in the direct

and indirect case of the $WO_{2.72}$:Fe thin films decreases by increasing the doping concentration. This would present a similar result for the nanowires of Ti doped $WO_{2.72}$ [30]. The bandgap of $WO_{2.72}$ is primarily formed by the 2p orbitals of oxygen, which constitute the valence band, and the 5d orbitals of tungsten, which constitute the conduction band. When iron is introduced, its 3d orbitals, which have energy levels situated between the valence and conduction bands, participate. The interaction between the 2p orbitals of oxygen, the 5d orbitals of tungsten, and the 3d orbitals of iron leads to the formation of new intermediate energy levels. This interaction results in the reduction of the effective bandgap [31].

Table 6. Energy band gaps and Urbach energy of $WO_{2.72}$:Fe thin films after annealing at 550 °C for 4 h

Fe-doping, %	E_g^I, eV	E_g^{II}, eV	E_u, meV
1	4.03	3.70	0.226
3	4.02	3.65	0.257
5	3.93	3.50	0.249

Figure 6(a) shows the *Ln α* plots of the absorption coefficient as a function of photon energy. In this region, called the Urbach region. The following relation gives the absorption coefficient:

$$\alpha = \alpha_0 \, exp(\frac{h\upsilon}{E_u}) \tag{9}$$

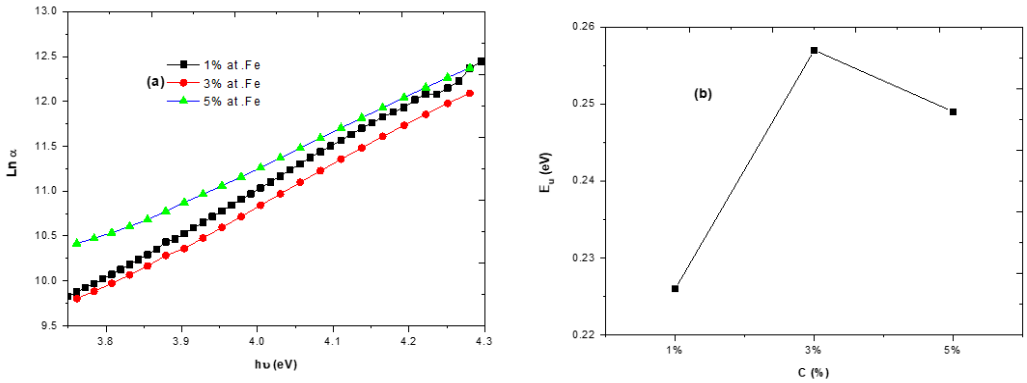

Fig. 6. Urbach energy determination (a) and values (b) of $WO_{2.72}$:Fe thin films

Therefore:

$$L\,n\,\alpha = L\,n\,\alpha_0 + \frac{h\upsilon}{E_u}, \tag{10}$$

where α_0 is a constant and E_u is the Urbach energy.

To measure the width of tail states, the Urbach energy E_u was calculated from the equation:

$$E_u = \left\{\frac{d(L\,n\,\alpha)}{d(h\upsilon)}\right\}^{-1}. \tag{11}$$

The Urbach energy values of $WO_{2.72}$:Fe thin films annealed at 550 °C for 4 hours are gathered in Table 6. Figure 6(b) shows the variation of the Urbach energy with Fe-doping. It is observed that E_u increases indicating the widening of the tail's states. Moreover, E_u is sensitive to disorder and the increase of the crystallinity in the films, which is believed to explain the variation, observed for the prepared thin films.

Conclusion

The Fe-doped $WO_{2.72}$ thin films were synthesized on glass substrates by the reactive chemical spraying technique in liquid phase (spray-pyrolysis) using ammonium tungstate $(NH_4)_{10}H_2(W_2O_7)_6$ as a precursor with a concentration 0.005 M. The dopant concentrations were 1, 3 and 5 % at. After deposition, the thin films were annealed at 550 °C for 4 h. The GIXRD analysis shows that all the samples obtained before the annealing are amorphous; on the other hand, the thin films obtained after annealing at 550 °C for 4 h are polycrystalline in nature, with a monoclinic structure of $WO_{2.72}$. The surface profiles are reduced by the increase of doping. The thickness of the $WO_{2.72}$:Fe thin films varies between 245 and 396 nm. The average grain size goes from 33.92 to 45.31 nm and 34.00 nm for Fe doping at 1, 3 and 5 %, respectively. The films obtained have a large number of defects such as oxygen vacancies, which are responsible for their high optical selectivity in the UV-Vis range. The films have direct and indirect electronic transitions, where the energy of the authorized indirect electronic transition is shifted to the red in all samples due to doping with Fe.

References

1. Kumar KN, Sattar SA, Ashok Reddy GV, Jafri RI, Premkumar R, Meera MR, Ahamed AA, Muthukrishnan M, Dhananjaya M, Tighezza AM. Structural, optical, and electrochromic properties of RT and annealed sputtered tungsten trioxide (WO_3) thin films for electrochromic applications by using GLAD technique. *Journal of Materials Science: Materials in Electronics*. 2023;34(28): 1934.
2. Nabeel MI, Hussain D, Ahmad N, Najam-ul-Haq M, Musharraf SG. Recent Advancements in Fabrication and Photocatalytic Applications of Graphitic Carbon Nitride-Tungsten Oxide Nanocomposites. *Nanoscale Advances*. 2023;5: 5214–5255.
3. Zeb S, Sun G, Nie Y, Xu H, Cui Y, Jiang X. Advanced developments in nonstoichiometric tungsten oxides for electrochromic applications. *Materials Advances*. 2021;2(21): 6839–6884.
4. Boruah PJ, Khanikar RR, Bailung H. Synthesis and characterization of oxygen vacancy induced narrow bandgap tungsten oxide (WO_{3-x}) nanoparticles by plasma discharge in liquid and its photocatalytic activity. *Plasma Chemistry and Plasma Processing*. 2020;40(4): 1019–1036.
5. Wu R, Cheng LH, Ma CQ, Yuan ZT, Song J. Enhancing the sensing performance of $WO_{2.72}$ toward n-butanol via loading CeO_2 nanoparticles. *Journal of Materials Chemistry A*. 2024;12(24): 5678–5687.
6. Qiu H, Chen Q, An X, Liu Q, Xie L, Zhang J, Yao W, Luo Y, Sun S, Kong Q, Chen J. WO_2 nanoparticles with oxygen vacancies: a high-efficiency electrocatalyst for the conversion of nitrite to ammonia. *Journal of Materials Chemistry A*. 2022;10(47): 24969–24974.
7. Zhang M, Sun H, Guo Y, Wang D, Sun D, Su Q, Ding S, Du G, Xu B. Synthesis of oxygen vacancies implanted ultrathin WO_{3-x} nanorods/reduced graphene oxide anode with outstanding Li-ion storage. *Journal of Materials Science*. 2021;56: 7573–7586.
8. Wu CM, Naseem S, Chou MH, Wang JH, Jian YQ. Recent advances in tungsten-oxide-based materials and their applications. *Frontiers in Materials*. 2019;6: 49.
9. Gutpa J, Shaik H, Kumar KN, Sattar SA. PVD techniques proffering avenues for fabrication of porous tungsten oxide (WO_3) thin films: A review. *Materials Science in Semiconductor Processing*. 2022;143: 106534.
10. Ouadah E, Hamdadou N., Ammari A. Morphological, Structural and Optical Properties of Fe-Doped WO_3 Films Deposited by Spray-Pyrolysis. *Journal of Electronic Materials*. 2022;51(1): 356–369.
11. Xi Z, Erdosy DP, Mendoza-Garcia A, Duchesne PN, Li J, Muzzio M, Li Q, Zhang P, Sun S. Pd nanoparticles coupled to $WO_{2.72}$ nanorods for enhanced electrochemical oxidation of formic acid. *Nano Letters*. 2017;17(4): 2727–2731.
12. Shang Y, Cui Y, Shi R, Yang P, Wang J, Wang Y. Regenerated $WO_{2.72}$ nanowires with superb fast and selective adsorption for cationic dye: Kinetics, isotherm, thermodynamics, mechanism. *Journal of Hazardous Materials*. 2019;379: 120834.

13. Kahattha C, Noonuruk R, Pecharapa W. Effect of titanium dopant on physical and optical properties of WO_3 thin films prepared by sol-gel method. *Suranaree Journal of Science & Technology*. 2019;26(1): 37–43.
14. Al-Kuhaili MF, Drmosh QA. Investigating the structural and optoelectronic properties of co-sputtered Fe-doped WO_3 thin films and their suitability for photocatalytic applications. *Materials Chemistry and Physics*. 2022;281: 125897.
15. Mak AK, Tuna Ö, Sezgin N, Üstün AM, Yılmaz Ş, Öztürk O, Karabulut M. Effect of Al do on the electrochromic properties of WO_3 thin films. *Thin Solid Films*. 2022;751: 139241.
16. Morankar PJ, Amate RU, Teli AM, Beknalkar SA, Chavan GT, Ahir NA, Jeon CW. Nanogranular advancements in molybdenum-doped tungsten oxide for superior electrochromic energy storage. *Journal of Energy Storage*. 2024;84: 110978.
17. Haroon A, Anwar K, Ahmed AS. Visible light-driven photo remediation of hazardous cationic dye via Ce-doped WO_3 nanostructures. *Journal of Rare Earths*. 2024;42(5): 869–878.
18. Shaheen N, Warsi MF, Zulfiqar S, Althakafy JT, Alanazi AK, Din MI, Abo-Dief HM, Shahid M. La-doped WO_3AgCN Nanocomposite for Efficient degradation of cationic dyes. *Ceramics International*. 2023;49(10): 15507–15526.
19. Chalotra S, Kaur P, Kaur S, Kandasami A, Kaur P, Singh DP. Influence of implantation assisted Ni do on structural and optical properties of $WO_{2.72}$ films. *Optical Materials*. 2023;136: 113479.
20. Wang JC, Shi W, Sun XQ, Wu FY, Li Y, Hou Y. Enhanced photo-assisted acetone gas sensor and efficient photocatalytic degradation using Fe-doped hexagonal and monoclinic WO_3 Phase– Junction. *Nanomaterials*. 2020;10(2): 398.
21. Habieb H, Hamdadou N. Preparation and characterization of undoped and antimony doped tin oxide thin films synthesized by spray pyrolysis. *Materials Physics and Mechanics*. 2022;48(3): 367–378.
22. John J, Pillai. S S, Philip R, Pillai VM. Effect of Fe doping on the structural, morphological, optical, magnetic and dielectric properties of $BaSnO_3$. *Journal of Materials Science: Materials in Electronics*. 2021;32: 11763–11780.
23. Bootchanont A, Phacheerak K, Fongkaew I, Limpijumnong S, Sailuam W. The pressure effect on the structural, elastic, and mechanical properties of orthorhombic $MgSiN_2$ from first-principles calculations. *Solid State Communications*. 2021;336: 114318.
24. Osiac M, Cioatera N, Jigau M. Structural, morphological, and optical properties of iron doped WO_3 Thin film prepared by pulsed laser deposition. *Coatings*. 2020;10(4): 412.
25. Reddy GV A, Naveen Kumar K, Sattar SA, Shetty HD, Guru Prakash N, Imran Jafri R, Devaraja C, Manjunatha BC, Kaliprasad CS, Premkumar R, Ansar S. Effect of post annealing on DC magnetron sputtered tungsten oxide (WO_3) thin films for smart window applications. *Physica B Condensed Matter*. 2023;664: 414996.
26. Taha TA, Ahmed EM, El-Tantawy AI, Azab AA. Investigation of the iron do on the structural, optical, and magnetic properties of Fe-doped ZnO nanoparticles synthesized by sol–gel method. *Journal of Materials Science: Materials in Electronics*. 2022;33(9): 6368–6379.
27. Gao H, Zhu L, Peng X, Zhou X, Qiu M. Fe-doped WO_3 nanoplates with excellent bifunctional performances: Gas sensing and visible light photocatalytic degradation. *Applied Surface Science*. 2022;592: 153310.
28. Kalanur SS. Structural, optical, band edge and enhanced photoelectrochemical water splitting properties of tin-doped WO_3. *Catalysts*. 2019;9(5): 456.
29. Betkar MM, Bagde GD. Structural and optical properties of spray deposited CdSe thin films. *Materials Physics and Mechanics*. 2012;14(1): 74–77.
30. İloğlu O, Yurtsever HA. The effects of annealing temperature on the thickness, morphology, band gap energy, and photocatalytic performance of ZIF-8-derived ZnO/TiO_2 thin films. *Journal of Materials Science: Materials in Electronics*. 2024;35(18): 1211.
31. Thirumoorthi G, Gnanavel B, Kalaivani M, Ragunathan A, Venkatesan H. Suitability of iron (Fe)-doped tungsten oxide (WO_3) nanomaterials for photocatalytic and antibacterial applications. *International Journal of Nanoscience*. 2021;20(05): 2150042.

About Authors

Elaid Ouadah
PhD, Researcher (Ecole Nationale Polytechnique d'Oran, Oran, Algérie)

Nasr Eddine Hamdadou
PhD, Professor (Ecole Nationale Polytechnique d'Oran, Oran, Algérie)